

# GRB 221009A Afterglow from a Shallow Angular Structured Jet

Ramandeep Gill<sup>1,3</sup>★ and Jonathan Granot<sup>2,3,4</sup>†

<sup>1</sup>*Instituto de Radioastronomía y Astrofísica, Universidad Nacional Autónoma de México, Antigua Carretera a Pátzcuaro # 8701, Ex-Hda. San José de la Huerta, Morelia, Michoacán, México C.P. 58089*

<sup>2</sup>*Department of Natural Sciences, The Open University of Israel, P.O. Box 808, Ra'anana 4353701, Israel*

<sup>3</sup>*Astrophysics Research Center of the Open University (ARCO), The Open University of Israel, P.O. Box 808, Ra'anana 4353701, Israel*

<sup>4</sup>*Department of Physics, The George Washington University, Washington, DC 20052, USA*

Accepted XXX. Received YYY; in original form ZZZ

## ABSTRACT

Exceptionally bright gamma-ray burst (GRB) afterglows can reveal the angular structure of their jets. GRB jets appear to have a narrow core (of half-opening angle  $\theta_c$ ), beyond which their kinetic energy drops as a power-law with angle  $\theta$  from the jet's symmetry axis,  $E_{k,\text{iso}}(\theta) \propto [1 + (\theta/\theta_c)^2]^{-a/2}$ . The power-law index  $a$  reflects the amount of mixing between the shocked jet and confining medium, which depends on the jet's initial magnetization. Weakly magnetized jets undergo significant mixing, leading to shallow ( $a \lesssim 2$ ) angular profiles. We use the exquisite multi-waveband afterglow observations of GRB 221009A to constrain the jet angular structure using a dynamical model that accounts for both the forward and reverse shocks, for a power-law external density profile,  $n_{\text{ext}} \propto R^{-k}$ . Both the forward-shock emission, that dominates the optical and X-ray flux, and the reverse-shock emission, that produces the radio afterglow, require a jet with a narrow core ( $\theta_c \approx 0.021$ ) and a shallow angular structure ( $a \approx 0.8$ ) expanding into a stellar wind ( $k \approx 2$ ). Moreover, these data appear to favor a small fraction ( $\xi_e \approx 10^{-2}$ ) of shock-heated electrons forming a power-law energy distribution in both shocks.

**Key words:** gamma-ray burst: general – stars:jets – relativistic processes

## 1 INTRODUCTION

New, paradigm-shifting insights into gamma-ray burst (GRB) physics can be gained by observing exceptionally bright GRBs, such as the recent GRB 221009A (An et al. 2023; Frederiks et al. 2023; Lesage et al. 2023; Ripa et al. 2023; Burns et al. 2023) that had an extremely high fluence of  $S_\gamma \sim 0.2 \text{ erg cm}^{-2}$ . This is a result of its relatively closer distance, with a redshift of  $z = 0.151$  (e.g. de Ugarte Postigo et al. 2022; Malesani et al. 2023), and a record-breaking prompt  $\gamma$ -ray isotropic equivalent energy release of  $E_{\gamma,\text{iso}} \sim 1.2 \times 10^{55} \text{ erg}$ , over a total duration of  $t_{\text{GRB}} \sim 600 \text{ s}$ . This GRB is even more important and unique since the Large High Altitude Air Shower Observatory (LHAASO) reported the detection of over 5000 very-high-energy photons, including an 18 TeV photon, within 2000 s of the burst trigger (Huang et al. 2022).

The broadband afterglow of this burst was recorded in exquisite detail from radio to  $\gamma$ -rays (Bright et al. 2023; Laskar et al. 2023; O'Connor et al. 2023; Fulton et al. 2023; Kann et al. 2023; An et al. 2023; Williams et al. 2023; Frederiks et al. 2023; Lesage et al. 2023). Its modeling in some of these works and others (Ren et al. 2022; Sato et al. 2023) with the canonical forward-shock (FS) and reverse-shock (RS) emission from a uniform and even a two-component jet presented some challenges. In particular, Laskar et al. (2023) found it difficult to explain the radio data both with the RS and FS afterglows in the wind ( $k = 2$ ) scenario (for an external medium density  $n_{\text{ext}} \propto R^{-k}$ ) which they preferred over the interstellar medium (ISM;  $k = 0$ )

case. In addition, their FS model could not adequately fit both the early- ( $\lesssim 1 \text{ day}$ ) and late-time ( $\gtrsim 30 \text{ day}$ ) optical data. Some success was achieved by O'Connor et al. (2023) who modeled the FS emission from a shallow angular structured jet and the RS emission from a spherical outflow expanding into a uniform medium (ISM).

The angular structure of the relativistic outflows in GRBs is challenging to constrain. An important step in this direction came with the discovery of the coincident detection of gravitational waves and short prompt GRB emission from the binary neutron star merger in GW170817 (Abbott et al. 2017), followed by a peculiar afterglow (e.g., Margutti et al. 2018; Troja et al. 2019). Hints of jet angular structure were also found in other GRBs (e.g. Racusin et al. 2008). An angular structure naturally forms as the jet bores its way through the confining medium near its launching site, i.e. the stellar envelope in long-soft GRBs and the binary merger ejecta in short-hard GRBs, as has been demonstrated with numerical simulations (e.g., Gottlieb et al. 2020, 2021; Nathanail et al. 2021). More importantly, the jet angular structure is sensitive to the amount of mixing that occurs during jet breakout, between the inner and outer cocoon (shocked jet material and confining medium). The amount of mixing is, in turn, strongly affected by the jet's initial magnetization, which remains poorly constrained and its knowledge is of paramount importance.

Afterglow emission arising from the FS for different jet angular structures have been calculated in several works (e.g. Rossi et al. 2002, 2004; Granot & Kumar 2003; Kumar & Granot 2003; Granot et al. 2005; Granot 2005; Gill & Granot 2018, 2020; Beniamini et al. 2020, 2022) with varying degree of sophistication. The reverse shock emission from such jets with angular structure was considered only in few works (Yan et al. 2007; Lamb & Kobayashi 2019). Here we

★ E-mail: r.gill@irya.unam.mx

† E-mail: granot@openu.ac.il

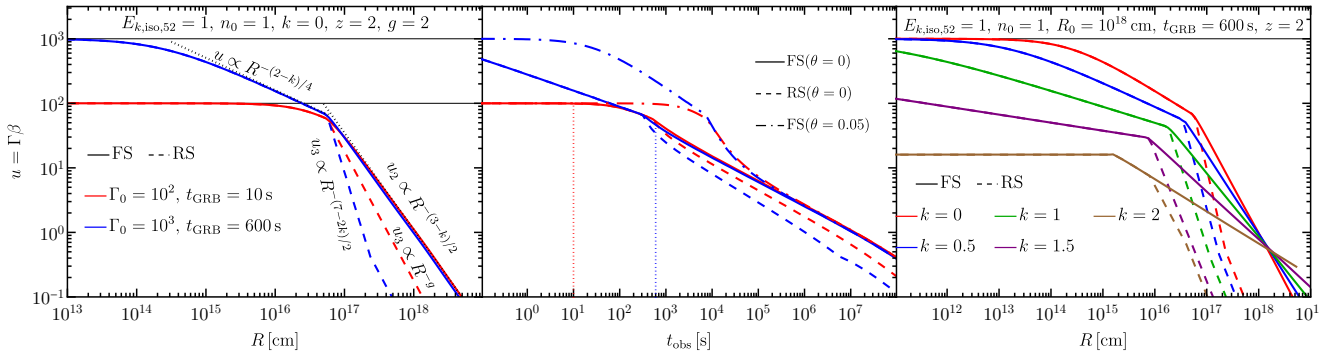


**Figure 1.** The proper speed  $u = \Gamma\beta$  of the shocked regions downstream of the forward (FS) and reverse (RS) shocks. **Left:** Two different prompt GRB durations  $t_{\text{GRB}}$  and initial bulk LFs  $\Gamma_0$  are chosen to obtain the thin-shell (red) and thick-shell (blue) cases. **Middle:** The same curves from the left panel are now shown as a function of the photon arrival time  $t_{\text{obs}}$  for an observer at  $\theta_{\text{obs}} = 0$  from emission by material moving along different  $\theta = \{0, 0.05\}$ . The two vertical lines show  $t_{\text{GRB}}$  (for  $\theta = 0$ ). **Right:** Proper speed evolution in the thick-shell case shown for different external medium density profiles,  $n_{\text{ext}} = n_0(R/R_0)^{-k}$  with  $\Gamma_0 = 10^3$ . The  $u_3$  of the RS-heated material changes slope as it transitions from having a relativistic (thick-shell) to a non-relativistic (thin-shell) temperature.

systematically consider the reverse shock emission from jets with angular structure, along with the system’s global RS-FS dynamics, which becomes important in the thick-shell regime (see §2).

The multi-wavelength afterglow observations of the exceptionally bright GRB 221009A present a golden opportunity to constrain the jet angular structure and its initial magnetization. We start by summarizing the analytic scalings for thin and thick shells in §2 for later comparison. In §3 we calculate the FS and RS dynamical evolution in an adiabatic spherical blast wave using our semi-analytical model. We extend this model to angular structured jets and obtain the afterglow emission from both shocks in §4. By comparing the emission to time-resolved spectra and lightcurve of GRB 221009A we demonstrate that its afterglow is produced by a jet with a shallow angular structure. The implications of our results are discussed in §5.

## 2 FORWARD-REVERSE SHOCK DYNAMICS

The self-similar dynamical evolution and radial structure of a relativistic spherical blast wave was first calculated by Blandford & McKee (1976, BM76 hereafter). It was used to explain the long-lasting and broad band afterglow emission of GRBs in several seminal works (e.g. Rees & Meszaros 1992; Meszaros & Rees 1993; Sari & Piran 1995). In this model, a cold baryonic spherical shell of (lab-frame) initial width  $\Delta_0$  and with kinetic energy  $E_{k,\text{iso}}$  coasting at an initial bulk-LF  $\Gamma_0$  is decelerated by sweeping up the surrounding external medium with number density  $n_{\text{ext}}(R) = n_0(R/R_0)^{-k}$ . In the process a double shock structure develops with four different regions (quantities in these regions have their respective labels): (1) the unshocked external medium, (2) the shocked external medium, (3) the shocked ejecta, and (4) the unshocked ejecta. Regions 2 and 3 are separated by a contact discontinuity (CD) and thus have the same pressure and LF,  $\Gamma_2 = \Gamma_3$ . A relativistic FS propagates into region 1 with bulk LF  $\Gamma_{\text{sh}} = \sqrt{2}\Gamma_2$ , shock heating the swept up external medium and accelerating it to a LF  $\Gamma_2$ . At the same time, a RS, which may either be relativistic (thick shell) or not (thin shell), propagates into the relativistic ejecta, shock heating and decelerating it.

The dynamical evolution of this adiabatically expanding system (Sari & Piran 1995; Kobayashi et al. 1999) depends on whether the reverse shock becomes relativistic before crossing the ejecta, the so called *thick-shell* scenario for which  $\Gamma_4 = \Gamma_0 > \Gamma_{\text{cr}}$ , or remains Newtonian (or becomes at least mildly relativistic) as in the *thin-shell* case for which  $\Gamma_0 < \Gamma_{\text{cr}}$ . The two regimes are separated by the critical LF (e.g., Kobayashi & Zhang 2003; Granot

& Ramirez-Ruiz 2012; Granot 2012),  $\Gamma_{\text{cr}} = (\ell/\Delta_0)^{(3-k)/2(4-k)}$ , where  $\ell \equiv (E_{k,\text{iso}}/Ac^2)^{1/(3-k)}$  is the Sedov length (ignoring order unity factors),  $A = m_p n_0 R_0^k$ , and  $m_p$  is the proton mass. The initial width of the shell can be inferred from  $\Delta_0 = (1+z)^{-1} ct_{\text{GRB}}$  for a prompt GRB of apparent duration  $t_{\text{GRB}}$  at a redshift  $z$ .

After the RS becomes relativistic in the thick-shell case, it starts to considerably reduce the ejecta’s bulk LF ( $\Gamma_3 \ll \Gamma_4$ ). During this time, the LF of the shocked material (contact discontinuity) is independent of  $\Gamma_0$  and obeys the scaling  $\Gamma_3 = \Gamma_2 \sim (L/Ac^3)^{1/4} R^{-(2-k)/4}$  (Sari 1997) where  $L = E_{k,\text{iso}}c/\Delta_0$  is the source’s (isotropic equivalent) kinetic power. After that, only a small fraction of the initial kinetic energy of the ejecta is extracted at a radius where the mass of the swept up external medium becomes comparable to  $M_0/\Gamma_0$ , with  $M_0 = E_{k,\text{iso}}/\Gamma_0 c^2$  being the baryon load of the ejecta. Most of this energy is extracted at the shock crossing radius,  $R_\Delta \sim R_{\text{cr}} \sim \Delta_0 \Gamma_{\text{cr}}^2$ , where the shocked ejecta and shocked external medium have comparable energies. Beyond  $R_{\text{cr}}$ , most of the initial kinetic energy of the ejecta resides in the shocked external medium while the fraction in the shocked ejecta rapidly declines. The evolution of the blast wave (FS) is then described by the self-similar BM76 solution such that  $\Gamma_2 \sim \Gamma_{\text{cr}}(R/R_{\text{cr}})^{-(3-k)/2} \sim (E_{k,\text{iso}}/Ac^2)^{1/2} R^{-(3-k)/2}$ . So long the shocked ejecta is relativistically hot (with adiabatic index  $\hat{\gamma} = 4/3$ ), its evolution is approximately consistent with the BM76 self-similar radial profile (Sari & Piran 1999a,b; Kobayashi et al. 1999; Kobayashi & Sari 2000), with  $\Gamma_3 \sim \Gamma_{\text{cr}}(R/R_{\text{cr}})^{-(7-2k)/2}$ . When the temperature of the shocked ejecta becomes non-relativistic, the BM76 solution no longer applies to it.

In the thin-shell case, the reverse shock never becomes relativistic. It is initially Newtonian and for a reasonable spread in the initial LF,  $\Delta\Gamma_0 \sim \Gamma_0$ , it starts spreading radially at  $R_s \sim \Delta_0 \Gamma_0^2$  with  $\Delta \sim \max(\Delta_0, R/\Gamma_0^2)$ , and becomes mildly relativistic near the crossing radius,  $R_\Gamma \sim (E_{k,\text{iso}}/Ac^2 \Gamma_0^2)^{1/(3-k)} \sim \ell \Gamma_0^{-2/(3-k)}$ . Therefore, at  $R_\Gamma$  we have  $\Gamma_3 = \Gamma_2 \approx \Gamma_0$ , the swept up mass is  $\sim M_0/\Gamma_0$ , and most of the kinetic energy is transferred to the shocked external medium. Beyond  $R_\Gamma$  the blast wave (FS) commences the BM76 self-similar evolution. Since the reverse shock never becomes relativistic, the shocked ejecta remains at a sub-relativistic temperature (with  $\hat{\gamma} = 5/3$ ). As a result, its evolution cannot be described by the BM76 solution after shock crossing. Assuming a power law with  $\Gamma_3(R) \propto R^{-g}$ , Kobayashi & Sari (2000) argued that  $3/2 \leq g \leq 7/2$  (or  $\frac{3-k}{2} \leq g \leq \frac{7-2k}{2}$  for a general  $k$ ) and showed that  $g \sim 2$  is consistent with one-dimensional hydrodynamical numerical simulations.

### 3 ADIABATIC SPHERICAL BLAST WAVES

Many works have considered the dynamical evolution of an impulsive relativistic blast wave undergoing adiabatic and/or radiative expansion (Blandford & McKee 1976; Katz & Piran 1997; Chiang & Dermer 1999; Piran 1999; Huang et al. 1999; Beloborodov & Uhm 2006; Pe'er 2012) mostly in the limit of a homogeneous shell where its radial structure is ignored. Most of these works have focused on the thin-shell scenario where the reverse shock contribution to the system dynamics is relatively modest. However, including the influence of the reverse shock on the system dynamics is crucial in the thick shell case, which is most relevant for many long GRBs, and makes the model more realistic in the thin shell case. Here we adopt the self-consistent model of Nava et al. (2013) (also see Zhang et al. 2022) that treats the entire dynamical evolution of an adiabatic/radiative blast wave and allows for an arbitrary density profile of the external medium. Below we only present its most salient features.

Consider a relativistic spherical shell of initial (lab-frame) thickness  $\Delta_0$ , bulk LF  $\Gamma_0$ , and mass loading  $M_0$  expanding into an external medium with number density  $n_{\text{ext}}(R)$ . The (lab-frame) total energy of the system is  $E_{\text{tot}} = \Gamma_0 M_{0,4} c^2 + \Gamma M_{0,3} c^2 + \Gamma m c^2 + \Gamma_{\text{eff},3} E'_{\text{int},3} + \Gamma_{\text{eff},2} E'_{\text{int},2}$  where  $\Gamma_4 = \Gamma_0$  and  $M_0 = M_{0,3} + M_{0,4}$ . During reverse-shock crossing it is assumed that both regions (2) and (3) are in pressure balance ( $P'_2 = P'_3$ ) and move with the same bulk LF ( $\Gamma_3 = \Gamma_2 \equiv \Gamma$ ). The total mass swept up by the blast wave as it propagates a radial distance  $R$  in an external medium with density  $n_{\text{ext}}(R) \propto R^{-k}$  is  $m(R) = [4\pi m_p / (3 - k)] R^3 n_{\text{ext}}(R)$  for  $k < 3$ . The comoving internal energy of the shocked material is given by  $E'_{\text{int}}$  and  $\Gamma_{\text{eff}} = (\hat{\gamma}\Gamma^2 - \hat{\gamma} + 1)/\Gamma$  is the appropriate LF to accurately describe the Lorentz transformation of the internal energy (Pe'er 2012). Here  $\hat{\gamma} = (4\Gamma_{ud} + 1)/3\Gamma_{ud} = 4/3(5/3)$  is the adiabatic index for a fluid with relativistic (non-relativistic) temperature and  $\Gamma_{ud} = \Gamma_u \Gamma_d (1 - \beta_u \beta_d)$  is the relative LF between the upstream and downstream material that have LFs  $\Gamma_{\{u,d\}} = (1 - \beta_{\{u,d\}}^2)^{-1/2}$ .

As the shell propagates an infinitesimal radial distance  $dR$ , its total energy changes by an amount  $dE_{\text{tot}} = dm c^2 + \Gamma_{\text{eff},2} dE'_{\text{rad}}$  that is a sum of the rest mass energy of the matter swept up over that interval,  $dm = 4\pi m_p R^2 n_{\text{ext}} dR$ , and the energy that is radiated away. For an adiabatic blast wave, radiative losses are negligible over the dynamical time, and therefore, the second term can be neglected. The change in the internal energy of the shocked material is a sum of three terms,  $dE'_{\text{int}} = dE'_{\text{sh}} + dE'_{\text{ad}} + dE'_{\text{rad}}$ . Here  $dE'_{\text{sh}} = (\Gamma_{ud} - 1) dM c^2$  is the random kinetic energy of the newly shocked material, where  $dM = dm$  for region (2) and  $dM = dM_{0,3}$  for region (3). The terms  $dE'_{\text{ad}}$  and  $dE'_{\text{rad}}$  represent the change in energy due to adiabatic and radiative losses (see Eq. (13) of Nava et al. (2013)). By taking the differential of  $E_{\text{tot}}$  and noticing that  $dM_{0,4} = -dM_{0,3}$ , the rate of change of the bulk LF of the shocked material can be obtained,

$$\frac{d\Gamma}{dR} = - \frac{(\Gamma_{\text{eff},2} + 1)(\Gamma - 1) \frac{dm}{dR} c^2 + \Gamma_{\text{eff},2} \frac{dE'_{\text{ad},2}}{dR}}{(M_{0,3} + m)c^2 + E'_{\text{int},2} \frac{d\Gamma_{\text{eff},2}}{d\Gamma} + E'_{\text{int},3} \frac{d\Gamma_{\text{eff},3}}{d\Gamma}} \quad (1)$$

$$- \frac{(\Gamma - \Gamma_0 - \Gamma_{\text{eff},3} + \Gamma_{\text{eff},3} \Gamma_{43}) \frac{dM_{0,3}}{dR} c^2 + \Gamma_{\text{eff},3} \frac{dE'_{\text{ad},3}}{dR}}{(M_{0,3} + m)c^2 + E'_{\text{int},2} \frac{d\Gamma_{\text{eff},2}}{d\Gamma} + E'_{\text{int},3} \frac{d\Gamma_{\text{eff},3}}{d\Gamma}}.$$

This equation needs to be supplemented by  $dM_{0,3}/dR$ , the rate at which ejecta mass is entering the reverse shock. The differential number of baryons shocked by the RS as it moves a (lab-frame) radial distance  $d\Delta$  into the ejecta is  $dN_4 = 4\pi R^2 n'_4 \Gamma_4 d\Delta$ . Here we explicitly assume that the width of the shocked region is much smaller than the radial distance of the blast wave, and therefore, both shocks are approximately at the same radius, such

that  $R_{\text{RS}} \sim R_{\text{FS}} = R$ . Conservation of baryon number dictates that  $d\Delta = (\beta_4 - \beta_3)(1 - \Gamma_4 n'_4 / \Gamma_3 n'_3)^{-1} dR$  (Sari & Piran 1995). Putting this all together yields the mass injection rate into region (3),  $dM_{0,3}/dR = 4\pi R^2 \rho'_4 \Gamma_0 (\beta_0 - \beta) \left(1 - \Gamma_0 \rho'_4 / \Gamma \rho'_3\right)^{-1}$  where  $\rho'_4 = M_0 / 4\pi R^2 \Delta \Gamma_0$  is the proper mass density of the ejecta shell that has lab-frame width  $\Delta = \max[\Delta_0, R/\Gamma_0^2]$ .

We solve the system of equations describing  $d\Gamma/dR$  and  $dM_{0,3}/dR$  using a fourth-order Runge-Kutta-Fehlberg (RK45) routine with adaptive step size. Until RS crossing  $\Gamma_3(R) = \Gamma_2(R) = \Gamma(R)$ , but after RS crossing the evolution of the shocked ejecta is prescribed to either have a BM76 profile (thick-shell), with  $u_3(R) = \Gamma_3(R)\beta_3(R) = u_\Delta(R/R_\Delta)^{-(7-2k)/2}$ , or a general power-law (thin-shell), with  $u_3(R) = u_\Delta(R/R_\Delta)^{-s}$ . The shock crossing radius ( $R_\Delta$ ) is determined by integrating the equation for  $dM_{0,3}/dR$  and by implementing the condition  $M_{0,3}(R_\Delta) = M_0$ , and the corresponding  $u_\Delta = u(R_\Delta)$  is obtained from the solution of Eq. (1).

The BM76 profile is strictly valid for a relativistically hot gas that has adiabatic index  $\hat{\gamma} = 4/3$ . As the flow expands, the comoving pressure and number density decline as  $P'_3 \propto R^{-2(13-2k)/3}$  and  $n'_3 \propto R^{-(13-2k)/2}$ . The sound speed in the comoving frame,  $c'_s/c = (\hat{\gamma}P'/w')^{1/2}$ , depends on the ratio  $w'/P' = (\rho'/P')c^2 + \hat{\gamma}/(\hat{\gamma} - 1)$  where  $w'$  is the enthalpy density. In the thick-shell case, the shocked gas is initially relativistically hot, which means that  $(\rho'_3/P'_3)c^2 \ll \hat{\gamma}/(\hat{\gamma} - 1)$  and therefore,  $c'_s/c = \sqrt{\hat{\gamma}_3 - 1} = 1/\sqrt{3}$ . The ratio  $\rho'_3/P'_3 \propto R^{(13-2k)/6}$  grows with radius, and as a result, a relativistically hot fluid will become non-relativistic. Therefore, we switch to the thin-shell evolution when  $(\rho'_3/P'_3)c^2 > \hat{\gamma}_3/(\hat{\gamma}_3 - 1) = 4$ .

In Fig. 1, we show the proper speed  $u = \Gamma\beta$  evolution of the shocked material downstream of both the RS and FS for a thin and thick shell (*left & middle* panels) and for different external medium density profiles in the thick shell case (*right* panel). We compare the asymptotic slopes of  $u(R)$  in different regimes with analytical results and find excellent agreement. The model evolves the bulk LFs of the shocked material downstream of both the shocks until the crossing radius  $R_\Delta$  and only for the material behind the FS thereafter. For  $R > R_\Delta$ , the  $u_3(R)$  profiles are manually prescribed. In the thick-shell case,  $u_3(R)$  shows a change in slope as the shocked material transitions from having a relativistic (thick-shell) to a non-relativistic (thin-shell) temperature.

### 4 THE AFTERGLOW OF GRB 221009A

We consider an ultra-relativistic outflow with a power-law angular structure to describe the afterglow of GRB 221009A. This type of structure has been obtained in numerical simulations of long (short) GRB jets penetrating out of the progenitor star (merger ejecta) (e.g. Gottlieb et al. 2021), and was successful in explaining the peculiar afterglow of GW 170817/GRB 170817A (e.g. Gill & Granot 2018).

Both the energy per unit solid angle,  $\epsilon(\theta) = dE(\theta)/d\Omega = E_{k,\text{iso}}(\theta)/4\pi$  where  $d\Omega$  is the element of the solid angle, and the initial bulk LF (minus one) are described by a power law at polar angle  $\theta$  (measured from the jet symmetry axis) larger than some core angle  $\theta_c$  (e.g., Granot & Kumar 2003)

$$\left\{ \frac{\epsilon}{\epsilon_c}, \frac{\Gamma_0(\theta) - 1}{\Gamma_c - 1} \right\} = \left[ 1 + \left( \frac{\theta}{\theta_{c,\{\epsilon,\Gamma\}}} \right)^2 \right]^{-\{a,b\}/2} \quad (2)$$

The core angle and power-law indices for the energy and bulk LF are allowed to be different. Here we apply our model of a spherical blast wave to an angular structured flow by assuming that every



$\theta_{\text{obs}}$	$E_{k,\text{iso},c}$	$\Gamma_c$	$n_0(R_0)$	$k$	$A_*$	$p_{\text{FS}}$	$\epsilon_{e,-2}^{\text{FS}}$	$\epsilon_{B,-4}^{\text{FS}}$	$\xi_{e,\text{FS}}$	$p_{\text{RS}}$	$\epsilon_{e,-2}^{\text{RS}}$	$\epsilon_{B,-4}^{\text{RS}}$	$\xi_{e,\text{RS}}$	$g$	$t_{\text{GRB}}$
0.02 rad	$2 \times 10^{55}$ erg	300	$0.1 \text{ cm}^{-3}$	2	0.33	2.4	1.0	1.0	0.01	2.03	8	10	0.01	1.3	500 s

**Table 1.** Model parameters. The external density is normalized at  $R_0 = 10^{18}$  cm ( $A_* = n_0 R_0^2 / 3 \times 10^{35} \text{ cm}^{-1}$ );  $(a, b, \theta_{c,\epsilon}, \theta_{c,\Gamma}) = (0.8, 0.3, 0.021, 0.016)$ .

angle  $\theta$  on the flow's surface evolves independently as if it were part of a spherical flow with kinetic energy  $E_{k,\text{iso}}(\theta)$  and initial LF  $\Gamma_0(\theta)$ . Its dynamical evolution is obtained by solving the equations used for the spherical flow but now on a grid of polar angles  $\theta$ . For simplicity and computational convenience we ignore lateral spreading, which becomes important as the outflow approaches the non-relativistic Sedov-Taylor phase. In Fig. 2 we show the angular structure of the outflow that was adopted in order to describe the afterglow of GRB 221009A.

To calculate the afterglow emission we adopt the treatment in Gill & Granot (2018) and assume for simplicity that it arises from an infinitely thin shell. The two shocks accelerate a fraction  $\xi_e$  of the total swept up electrons into a power-law energy distribution with  $dn'_e/d\gamma_e \propto \gamma_e^{-p}$  (for  $\gamma_e > \gamma_m$ ), where  $n'_e$  is the number density of the synchrotron emitting electrons and  $\gamma_e$  is their LF. These electrons receive a fraction  $\epsilon_e$  of the total internal energy of the shocked gas, whereas a fraction  $\epsilon_B$  of the same goes into generating the small scale magnetic field that leads to synchrotron cooling. At a given observed time  $t_{\text{obs}}$ , the emission is obtained by integrating over the equal-arrival-time surface (EATS). We obtain smoother and more realistic spectral breaks in the comoving spectrum by adopting the smoothing prescription introduced in Granot & Sari (2002) for  $k = \{0, 2\}$  and later generalized to  $0 \leq k \leq 2$  in Leventis et al. (2012).

We find that the viewing angle of the observer is comparable to the core angle of the energy profile,  $\theta_{\text{obs}} \sim \theta_{c,\epsilon}$ , which is needed in order to explain the high fluence of the  $\gamma$ -ray emission and the multi-wavelength lightcurve. In contrast to some works (e.g. O'Connor et al. 2023), we find  $k \approx 2$  to avoid overproducing the sub-mm flux by the FS emission. The kinetic energy of the bipolar outflow in our model is  $E_k \propto \theta_F^{2-a} \propto t_{\text{obs}}^{\frac{(2-a)(3-k)}{(8-2k-a)}} \approx 4.2 \times 10^{52} (t_{\text{obs}}/100 \text{ days})^{0.375}$  erg for no jet break at  $t_{\text{obs}} < 100$  days (see Beniamini et al. 2022, for scalings), with  $E_{k,\text{max}} \approx 7 \times 10^{53}$  erg for a maximum jet angular size of  $\theta_{\text{max}} = 1$  rad. All the model parameters adopted for the FS and RS regions are shown in Table 1. These illustrate one possible approximate solution, while significant degeneracy remains.

The left panel of Fig. 4 compares the model spectra with multi-wavelength afterglow observations of GRB 221009A at different times and the right panel shows the corresponding comparison to the lightcurve. The X-ray afterglow is completely dominated by the FS emission at all times. The optical afterglow is initially RS dominated, at  $t_{\text{obs}} \lesssim 0.1$  days, and then becomes increasingly FS dominated. The RS emission also becomes highly suppressed at higher frequencies as the cut-off frequency ( $\nu_{\text{cut}}$ ) passes through the optical band towards even lower frequencies over time. The emission is not completely suppressed at  $\nu > \nu_{\text{cut}}$ , as one would expect from analytic models that only account for emission along the line-of-sight (LOS). Due to integration over the EATS, high-latitude emission coming from angles  $|\theta - \theta_{\text{obs}}| > 1/\Gamma(\theta_{\text{obs}})$  and which was emitted at earlier lab-frame times, when  $\nu_{\text{cut}} > \nu$ , makes a dominant contribution to the total flux over that emitted along the LOS. This effect will be described in a future publication (Gill & Granot, in preparation).

The middle panel of Fig. 4 compares the model spectra to the radio afterglow data from Laskar et al. (2023). The RS emission clearly dominates the radio flux at all times, with significant FS contribution

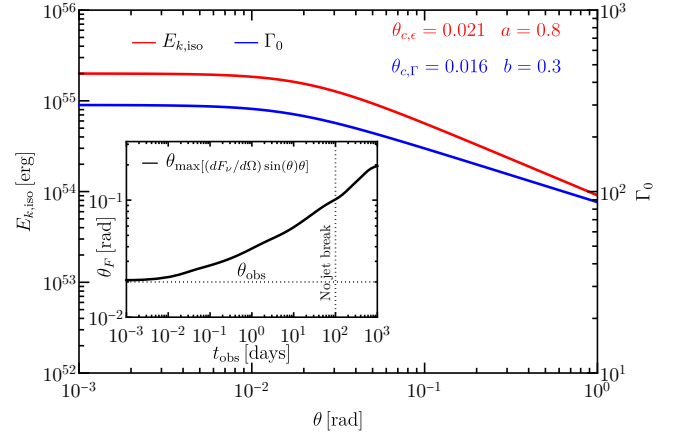


**Figure 2.** Angular structure of the outflow, showing the isotropic-equivalent (total) kinetic energy and initial bulk LF profiles as a function of polar angle  $\theta$  measured from the jet symmetry axis. The inset shows the temporal evolution of the polar angle  $\theta_F$  that dominates the X-ray flux, where the latter has shown no steepening due to a jet break at  $t_{\text{obs}} < 100$  days.

to the sub-millimeter flux coming in at late times. The RS radio emission is also self-absorbed below the self-absorption frequency, which decreases with time.

Our model is able to describe the multi-wavelength lightcurve reasonably well. In fact, the FS dominated X-ray lightcurve compares remarkably well with the data over a wide range of timescales and captures the shallow break around  $t_{\text{br}} \sim 0.8$  days. This break is caused by the shallow break in the energy profile at  $\theta \sim 0.04$  rad, emission from which angle dominates the flux at  $t_{\text{obs}} = t_{\text{br}}$  (see inset in Fig 2). A similar conclusion was reached in O'Connor et al. (2023). At  $t_{\text{obs}} \lesssim 0.3$  days,  $\nu_{\text{opt}} < \nu_m$  and therefore the FS lightcurve is expected to be flat when  $k = 2$ . This means that the slowly decaying optical flux at early times must come from a diminishing RS contribution. The radio data, which is completely dominated by emission from the RS, is explained well by our model at  $t_{\text{obs}} \gtrsim 1$  day. At earlier times, it over predicts the radio flux by a factors of a few when compared with the radio data from Bright et al. (2023). The origin of this discrepancy may lie in the rather coarse exploration of parameter space degeneracies conducted here. This can be addressed more efficiently using a simpler and computationally less intense parameterized model (e.g., Lamb & Kobayashi 2019).

## 5 CONCLUSIONS

We have explored a potential solution of emission from a jet with a shallow angular profile, both in energy ( $a \approx 0.8$ ) and initial bulk LF ( $b \approx 0.3$ ), to explain the multi-wavelength afterglow of the exceptionally bright GRB 221009A. In this model, the radio emission is attributed to that arising from the RS heated ejecta while the optical and X-ray flux is coming from the FS heated external medium.

We find that the data appear to favor that only a small ( $\xi_e \approx 10^{-2}$ ) fraction of shock-heated electrons are accelerated to a power-law energy distribution in both shocks. Similar, but somewhat larger,

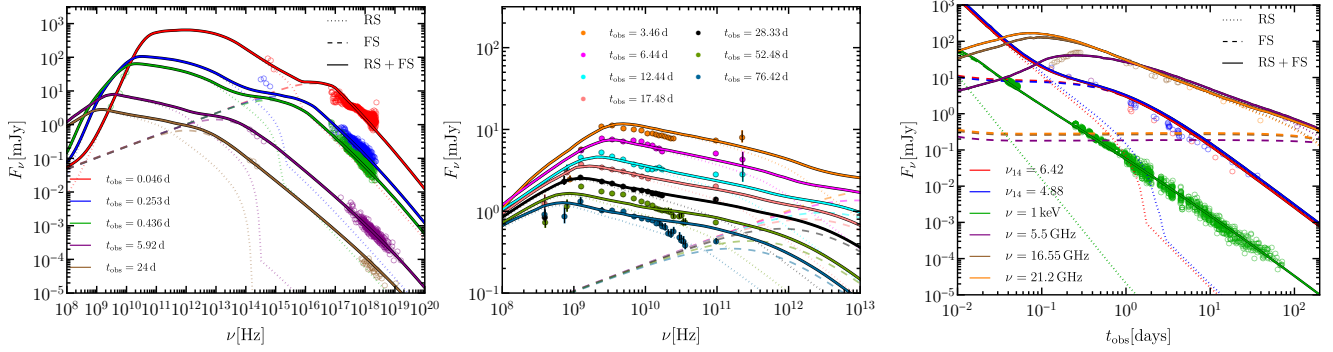


**Figure 3.** *Left:* Comparison of model spectra with the multi-wavelength afterglow of GRB 221009A from radio to X-rays at different observed times  $t_{\text{obs}}$  (measured from the GRB trigger time). *Middle:* Model comparison to the radio data from Laskar et al. (2023). The total emission is shown with solid lines while the reverse shock (RS) and forward shock (FS) components are shown with dotted and dashed lines, respectively. *Right:* Model comparison to the multi-wavelength lightcurve. The X-ray data is from *Swift*/XRT, and the optical and radio data are from O'Connor et al. (2023); Bright et al. (2023).

fractions have been obtained in other works (e.g. Salafia et al. 2022) and such a result is consistent with particle-in-cell simulations of magnetized collisionless shocks (Sironi & Spitkovsky 2011).

This is the first GRB in which clear hints for a shallow ( $a \lesssim 2$ ) structured outflow have been found. One of the key observations is the presence of a shallower achromatic break in the lightcurve ( $F_\nu \propto t_{\text{obs}}^\alpha$ ) with  $\Delta\alpha \sim 0.14$  at  $t_{\text{obs}} \sim 0.8$  days as compared to  $\Delta\alpha = \frac{3-k}{4-k} = 0.75$  (0.5) for  $k = 0$  (2), the jet-break expected in a non-spreading sharp-edged jet. O'Connor et al. (2023) pointed out several other bright jet-break-less GRBs that may be explained using the model explored here. If true, it may offer strong support for weakly magnetized jets in at least some long-soft GRBs (Bromberg & Tchekhovskoy 2016) as they break out from the stellar envelope, leading to more mixing and a shallow energy angular profile ( $a \lesssim 2$ ).

## ACKNOWLEDGEMENTS

R.G. acknowledges financial support from the UNAM-DGAPA-PAPIIT IA105823 grant, Mexico. J.G. acknowledges financial support by the ISF-NSFC joint research program (grant no. 3296/19).

## DATA AVAILABILITY

The model data can be shared upon reasonable request to the authors.

## REFERENCES

Abbott B. P., et al., 2017, *Physical Review Letters*, **119**, 161101  
 An Z.-H., et al., 2023, *arXiv e-prints*, p. arXiv:2303.01203  
 Beloborodov A. M., Uhm Z. L., 2006, *ApJ*, **651**, L1  
 Beniamini P., Granot J., Gill R., 2020, *MNRAS*, **493**, 3521  
 Beniamini P., Gill R., Granot J., 2022, *MNRAS*, **515**, 555  
 Blandford R. D., McKee C. F., 1976, *Physics of Fluids*, **19**, 1130  
 Bright J. S., et al., 2023, *arXiv e-prints*, p. arXiv:2303.13583  
 Bromberg O., Tchekhovskoy A., 2016, *MNRAS*, **456**, 1739  
 Burns E., et al., 2023, *ApJ*, **946**, L31  
 Chiang J., Dermer C. D., 1999, *ApJ*, **512**, 699  
 Frederiks D., et al., 2023, *arXiv e-prints*, p. arXiv:2302.13383  
 Fulton M. D., et al., 2023, *arXiv e-prints*, p. arXiv:2301.11170  
 Gill R., Granot J., 2018, *MNRAS*, **478**, 4128  
 Gill R., Granot J., 2020, *MNRAS*, **491**, 5815  
 Gottlieb O., Bromberg O., Singh C. B., Nakar E., 2020, *MNRAS*, **498**, 3320  
 Gottlieb O., Nakar E., Bromberg O., 2021, *MNRAS*, **500**, 3511  
 Granot J., 2005, *ApJ*, **631**, 1022  
 Granot J., 2012, *MNRAS*, **421**, 2442  
 Granot J., Kumar P., 2003, *ApJ*, **591**, 1086

Granot J., Ramirez-Ruiz E., 2012, Jets and GRB unification schemes  
 Granot J., Sari R., 2002, *ApJ*, **568**, 820  
 Granot J., Ramirez-Ruiz E., Perna R., 2005, *ApJ*, **630**, 1003  
 Huang Y. F., Dai Z. G., Lu T., 1999, *MNRAS*, **309**, 513  
 Huang Y., Hu S., Chen S., Zha M., Liu C., Yao Z., Cao Z., Experiment T. L., 2022, GRB Coordinates Network, 32677, 1  
 Kann D. A., et al., 2023, *arXiv e-prints*, p. arXiv:2302.06225  
 Katz J. I., Piran T., 1997, *ApJ*, **490**, 772  
 Kobayashi S., Sari R., 2000, *ApJ*, **542**, 819  
 Kobayashi S., Zhang B., 2003, *ApJ*, **582**, L75  
 Kobayashi S., Piran T., Sari R., 1999, *ApJ*, **513**, 669  
 Kumar P., Granot J., 2003, *ApJ*, **591**, 1075  
 Lamb G. P., Kobayashi S., 2019, *MNRAS*, **489**, 1820  
 Laskar T., et al., 2023, *ApJ*, **946**, L23  
 Lesage S., et al., 2023, *arXiv e-prints*, p. arXiv:2303.14172  
 Leventis K., van Eerten H., Meliani Z., Wijers R., 2012, *MNRAS*, **427**, 1329  
 Malesani D. B., et al., 2023, *arXiv e-prints*, p. arXiv:2302.07891  
 Margutti R., et al., 2018, *ApJ*, **856**, L18  
 Meszaros P., Rees M. J., 1993, *ApJ*, **405**, 278  
 Nathanail A., Gill R., Porth O., Fromm C. M., Rezzolla L., 2021, *MNRAS*, **502**, 1843  
 Nava L., Sironi L., Ghisellini G., Celotti A., Ghirlanda G., 2013, *MNRAS*, **433**, 2107  
 O'Connor B., et al., 2023, *arXiv e-prints*, p. arXiv:2302.07906  
 Pe'er A., 2012, *ApJ*, **752**, L8  
 Piran T., 1999, *Phys. Rep.*, **314**, 575  
 Racusin J. L., et al., 2008, *Nature*, **455**, 183  
 Rees M. J., Meszaros P., 1992, *MNRAS*, **258**, 41  
 Ren J., Wang Y., Zhang L.-L., Dai Z.-G., 2022, *arXiv:2210.10673*,  
 Ripa J., et al., 2023, *arXiv e-prints*, p. arXiv:2302.10047  
 Rossi E., Lazzati D., Rees M. J., 2002, *MNRAS*, **332**, 945  
 Rossi E., Lazzati D., Salmonson J. D., Ghisellini G., 2004, *MNRAS*, **354**, 86  
 Salafia O. S., et al., 2022, *ApJ*, **931**, L19  
 Sari R., 1997, *ApJ*, **489**, L37  
 Sari R., Piran T., 1995, *ApJ*, **455**, L143  
 Sari R., Piran T., 1999a, *ApJ*, **517**, L109  
 Sari R., Piran T., 1999b, *ApJ*, **520**, 641  
 Sato Y., Murase K., Ohira Y., Yamazaki R., 2023, *MNRAS*,  
 Sironi L., Spitkovsky A., 2011, *ApJ*, **726**, 75  
 Troja E., et al., 2019, *MNRAS*, **489**, 1919  
 Williams M. A., et al., 2023, *arXiv e-prints*, p. arXiv:2302.03642  
 Yan T., Wei D.-M., Fan Y.-Z., 2007, *Chinese J. Astron. Astrophys.*, **7**, 777  
 Zhang Z.-L., Liu R.-Y., Geng J.-J., Wu X.-F., Wang X.-Y., 2022, *MNRAS*, **513**, 4887  
 de Ugarte Postigo A., et al., 2022, GRB Coordinates Network, 32648, 1

This paper has been typeset from a  $\text{\LaTeX}$  file prepared by the author.